IAHR AIRH

Journal of Hydraulic Research Vol. 41, No. 3 (2003), pp. 271–284

Time evolution of scouring downstream of bed sills

Evolution en temps de l'affouillement à l'aval des seuils

ROBERTO GAUDIO, *Research Engineer, CNR-IRPI, Section of Cosenza, Via Cavour, 4–6, 87030 Rende (CS), Italy*

ANDREA MARION, *Assistant Professor, Department of Hydraulic, Maritime and Geotechnical Engineering, University of Padua, Via Loredan 20, 35131 Padua, Italy*

ABSTRACT

Results of laboratory experiments conducted on time evolution of the scouring phenomenon at bed sills are presented. Starting from previous findings on long-term depth and length of the local scour hole downstream of bed sills, 12 long-duration tests were designed and performed in the *Sloping Sediment Duct* at HR Wallingford Ltd., using uniform sand. No sediment feeding system was adopted. Video-recordings of the scour holes through the glass-sided duct allowed successive image analysis to obtain water surface and bed profiles over time.

Results confirmed the validity of the assessment method of the maximum scour depth, y_s, at equilibrium; uncertainties arose about the length of the scour hole, l_s. A cyclic phenomenon perturbing the scour hole was also observed and described. The investigation of the time evolution of y_s showed that the scour hole develops rapidly and conditions close to equilibrium are achieved in a short time. The introduction of a morphological time, t_s, permitted the non-dimensional description of the increasing of y_s over time through a unique curve. The short- and the long-term local scour regions are clearly distinguished. An application of the results is shown in a numerical example.

RÉSUMÉ

On présente des résultats d'expériences de laboratoire sur l'évolution dans le temps de l'affouillement au niveau des seuils. À partir de précédents résultats sur la profondeur et la longueur à long terme de la fosse locale d'affouillement en aval des seuils, 12 essais de longue durée ont été conçus et réalisés dans le canal en pente à lit mobile de HR Wallingford Ltd, en utilisant un sable uniforme. Aucun système d'alimentation en sédiments n'a été utilisé. Les enregistrements vidéo des fosses d'affouillement prises à travers les parois vitrées du canal ont permis, par l'analyse des images successives, d'obtenir l'évolution en temps des profils de la surface de l'eau et de celle du lit. Les résultats ont confirmé la validité de la méthode d'évaluation de la profondeur maximum d'affouillement, y_s, à l'équilibre ; des incertitudes ont surgi au sujet de la longueur de l'affouillement, l_S. Un phénomène cyclique perturbant la fosse a également été observé et décrit. La recherche sur l'évolution en temps de y_s a montré que l'affouillement se développe rapidement et que des conditions proches de l'équilibre sont réalisées en peu de temps. L'introduction d'un temps morphologique t_s, a permis la description adimensionnelle de l'évolution en temps de y_s par une courbe unique. Les régions d'affouillements locaux à long et court terme sont clairement distinguées. Une application des résultats est faite dans un exemple numérique.

Keywords: Bed sills; local scouring; time evolution.

1 Introduction

Bed sills are a common solution to stabilise degrading bed rivers and channels. Their presence limits the general erosion process, but also causes a local scouring phenomenon, by which the structure itself (and many times other structures in proximity of it, like bridge piers or abutments, or bank revetments) might be undermined.

A previous experimental work carried out in the *Tilting Flume* at HR Wallingford Ltd. [5] was devoted to the prediction of the equilibrium dimensions (maximum depth, y_s, and length, l_s) of the scour hole, occurring downstream of each sill. In the absence of sediment feeding (clear water conditions) and using two different uniform sediments (gravel of median grain size, respectively, $D_{50} = 8.5$ mm and 4.1 mm), the following empirical relations were obtained:

$$\frac{y_s}{H_s} = 0.189\frac{a_1}{\Delta D_{50}} + 0.266 \tag{1}$$

$$\frac{l_s}{H_s} = 1.87\frac{a_1}{\Delta D_{50}} + 4.02 \tag{2}$$

where $H_s = 1.5\sqrt[3]{q^2/g}$ is the critical specific energy in proximity of the sill, q is the discharge per unit width, g is the gravity acceleration, $a_1 = (S_0 - S_{eq})L$ is the morphological jump, S_0 and S_{eq} are, respectively, the initial and equilibrium longitudinal bed slope, L is the distance between two successive sills, $\Delta = \rho_s'/\rho_w$ is the relative submerged particle density, ρ_s' and ρ_w are, respectively, the submerged sediment and water density. Equations (1)

Revision received July 17, 2002. Open for discussion till October 31, 2003.

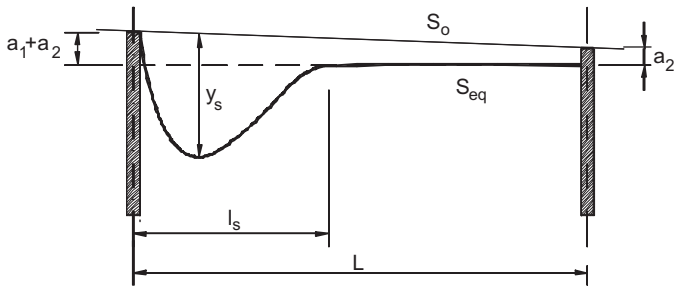

Figure 1 Definition sketch of scour at bed sills (from Gaudio *et al*., 2000).

and (2) are both valid in the range $1.3 \leq a_1/(\Delta D_{50}) \leq 9.1$, with a correlation coefficient $r = 0.98$. They show that the scour hole dimensions increase if discharge or morphological jump (i.e. difference between initial and equilibrium slope and/or distance between sills) increase, and if particle density or size decrease.

The presence of a step, a_2 (Figure 1), upstream of each sill was also observed and discussed, and the following expressions were proposed to assess its values [5]:

$$a_2 = h_u - h_c \quad \text{for} \quad \frac{a_2}{h_u} > 0.15, \tag{3}$$

$$q = \frac{2}{3}\sqrt{2g}\left(0.605 + \frac{0.001}{h_u - a_2} + 0.08\frac{h_u - a_2}{a_2}\right)(h_u - a_2)^{3/2} \quad \text{for} \quad \frac{a_2}{h_u} \leq 0.15, \tag{4}$$

where h_u is the normal flow depth. Equation (3) indicates that the value of the sill step, a_2, is simply given by the difference between the normal and the critical depths; Eq. (4) is Rehbock's implicit formula for low weirs, valid for $0.01 < (h_u - a_2) < 0.80$ m, with h_u and a_2 expressed in metres [6].

For practical purposes, designers are often interested in short-term local scouring. For instance, they are often required to predict the maximum scour depth at sills in the proximity of bridges when a flood occurs. Therefore, the investigation of the time evolution of a scour hole might provide the knowledge of short-term depth and length values, through a comparison with long-term ones. This was the main reason for performing a set of experimental tests in a hydraulics laboratory.

2 Experiments

The experimental work on time evolution of scouring downstream of bed sills included 12 tests. They were performed in the *Sloping Sediment Duct* at HR Wallingford Ltd., in 1998. The duct consists of a 6.75 m-long test section and its support cage, pivoting on a central support. The working length of the duct is 5.57 m. The test section presents a 60 cm-wide and 24.5 cm-high rectangular cross-section. Three parts of both side walls have glass panels, useful for the direct observation of the flow and sediment transport process. For the full description of the duct, see Damgaard *et al*. [2]. The upper part of the duct, i.e. the top cover of the cross-section, was removed to permit free surface flow (Figure 2).

Figure 2 *Sloping Sediment Duct*, HR Wallingford Ltd., 1998.

A recirculating pipe system was used: a centrifugal pump raised the water from a sump to the upstream end of the duct, producing a maximum velocity of about 1 m/s; at the outlet the discharge flowed into a tank, from which it went back to the sump through a return pipe. The discharge was measured using an Endress & Hauser electromagnetic flowmeter, positioned on the feeder pipework and linked to a Personal Computer.

The bed sills used in all experiments were 25 mm-thick by 15 cm-high wooden plates, with the same width as the transversal section. The first and second sills were located respectively at the longitudinal abscissa (starting from the inlet) $x = 2.00$ m and $x = 4.50$ m; the distance between sills, L, was therefore constantly equal to 2.50 m . A third sill was positioned at $x = 5.50$ m, very close to the outlet, and the reach between 4.50 and 5.50 m was used to collect eroded sediments, preventing them from reaching the tank and the water recirculating system. Periodic removal of the collected material avoided backwater effects and disturbances of the upstream hydrodynamic conditions.

The sediment used in all tests was sand; its grain-size distribution curve is shown in Figure 3, with median sediment diameter $D_{50} = 1.8$ mm and relative submerged particle density $\Delta = 1.63$. Since the uniformity coefficient $C_u = D_{60}/D_{10} = 1.4$ is less than 2, the sand can be considered as uniform [8]. In each run the sand was positioned in the reach $x = 0$ to 4.50 m, up to the same height as the top face of the sills, in order to form a flat bed. No sediment recirculating system was adopted.

An electronically indicating point gauge with acoustic device, with resolution and accuracy of ± 0.1 mm, was mounted on a gantry manually moving on rails placed above the side walls of the duct.

A video-camera was located on the support cage to record the time evolution of the scour hole through the glass panel at the left side of the duct downstream of the first sill. A monitor and a video-recorder were set to observe and record the local scouring phenomenon.

Particular care was addressed to the duct inlet: a honeycomb was inserted and cobbles were used to dissipate the eddy energy and to prevent secondary currents, so that an artificial boundary

layer could be created and quite uniform flow could take place in a short reach.

Tests were designed not only to study the time evolution of scouring, but also to verify the validity of Eqs. (1) and (2) in the same range of $a_1/(\Delta D_{50})$ with a different sediment. Therefore, initial slope and discharge were chosen in order to obtain desired values of the above dimensionless parameter. It was not possible to tilt the duct at high slope values, due to the fact that excessive scour depth would have occurred.

In each test the duct was tilted and the longitudinal slope was computed by measuring the depths of the top faces of the first and second sill with respect to the horizontal surface of still water stored in the duct. This operation was repeated until the required S_0 was obtained. A 20 cm-high sill was put at the outlet as a tailgate for the achievement of hydrostatic conditions. The water was pumped into the duct while slowly increasing the discharge (with the tailgate in place) to avoid sediment transport before the design value was reached. Once the correct flow rate was measured, the tailgate was removed and the test started.

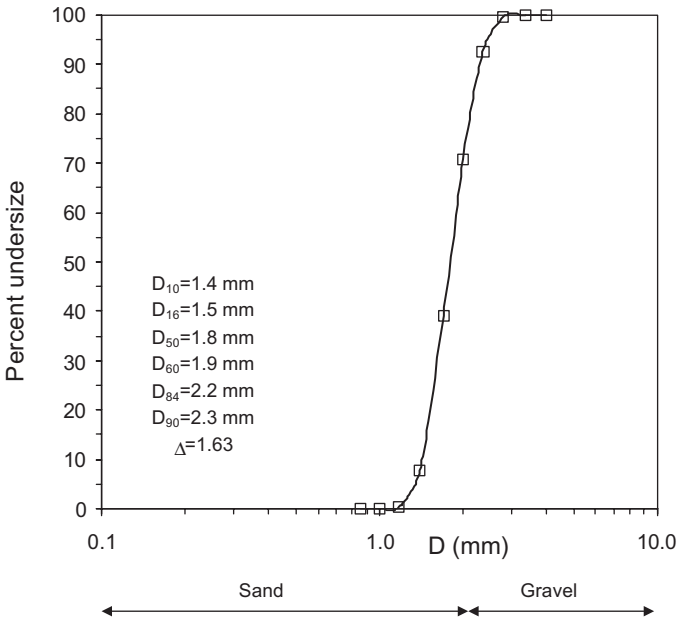

Figure 3 Grain-size distribution curve of the sediment used in tests.

All the tests lasted long enough to reach equilibrium conditions. Recordings of each test were performed with a time lapse video-recorder, able to record for 6 s and pause for 3 min; therefore, it was possible to store a 90 h-long run in a 3 h-long video-cassette.

Direct observation of the scour hole with the monitor showed that the final depth of the scour hole was always achieved in a few hours; conversely, the final value of the length seemed to need much longer time to be reached. When the bed profiles did not show significant variations, the tests were concluded and measurements of water surface and bed profiles were taken with the point gauge along the centreline.

Table 1 reports the independent variables of the tests: the width of the rectangular cross-section, B, the spacing between two successive sills, L, the median sediment size, D_{50}, the grain size for which 90% by weight of the sediment is finer, D_{90}, the relative submerged particle density, Δ, the discharge, Q, the discharge per unit width, q, the initial bed slope, S_0; in addition, the total duration, T, is shown. The dependent physical quantities are listed in Table 2: the Manning roughness coefficient, $n = D_{90}^{1/6}/26$, the normal flow depth, h_u, the equilibrium slope, S_{eq}, the critical flow depth, $h_c = \sqrt[3]{q^2/g}$, the critical specific energy, $H_s = 1.5h_c$, the morphological jump, a_1, the sill step according to Eq. (3), a_2, the sill step according to Eq. (4), $a_{2,Reb}$, the mean velocity, $U = q/h_u$, the Froude number, $Fr = U/(gh_u)^{0.5}$, the Reynolds number, $Re \approx 4h_uU/\nu$ where ν is the kinematic water viscosity assumed equal to 10^{-6} m^2/s , the shear velocity, $u^* = (gh_uS_{eq})^{0.5}$, the shear Reynolds number, $Re^* = u^*D_{50}/\nu$. Values of h_u and S_{eq} were computed according to the following expressions [5]:

$$h_u = \frac{(nq)^{6/7}}{(\Theta_c \Delta D_{50})^{3/7}}, \tag{5}$$

$$S_{eq} = \frac{(\Theta_c \Delta D_{50})^{10/7}}{(nq)^{6/7}}, \tag{6}$$

derived from the Manning uniform flow formula [9] and the Shields incipient motion condition [13]. The critical Shields mobility parameter, Θ_c, was chosen equal to 0.040, based on previous observations.

Table 1 Initial conditions and total duration of tests.

Test	B (m)	L (m)	D_{50} (m)	D_{90} (m)	Δ	Q (m^3/s)	q (m^2/s)	S_0	T (h)
1	0.60	2.5	0.0018	0.0023	1.63	0.0122	0.020	0.0094	88
2	0.60	2.5	0.0018	0.0023	1.63	0.0189	0.032	0.0070	70
3	0.60	2.5	0.0018	0.0023	1.63	0.0123	0.021	0.0071	88
4	0.60	2.5	0.0018	0.0023	1.63	0.0151	0.025	0.0063	45
5	0.60	2.5	0.0018	0.0023	1.63	0.0124	0.021	0.0062	69
6	0.60	2.5	0.0018	0.0023	1.63	0.0170	0.028	0.0059	70
7	0.60	2.5	0.0018	0.0023	1.63	0.0179	0.030	0.0102	51
8	0.60	2.5	0.0018	0.0023	1.63	0.0124	0.021	0.0102	89
9	0.60	2.5	0.0018	0.0023	1.63	0.0144	0.024	0.0110	60
10	0.60	2.5	0.0018	0.0023	1.63	0.0180	0.030	0.0110	66
11	0.60	2.5	0.0018	0.0023	1.63	0.0162	0.027	0.0084	70
12	0.60	2.5	0.0018	0.0023	1.63	0.0121	0.020	0.0084	90

Table 2 Calculated quantities.

Test	n (s/m$^{1/3}$)	h_u (m)	S_{eq}	h_c (m)	H_s (m)	a_1 (m)	a_2 (m)	$a_{2,Reb}$ (m)	U (m/s)	Fr	Re	u^* (m/s)	Re^*
1	0.014	0.044	0.0027	0.035	0.052	0.017	0.009	0.008	0.461	0.70	81333	0.034	61
2	0.014	0.064	0.0018	0.047	0.070	0.013	0.018	0.013	0.491	0.62	126000	0.034	61
3	0.014	0.044	0.0026	0.035	0.052	0.011	0.009	0.008	0.461	0.70	82000	0.034	61
4	0.014	0.053	0.0022	0.040	0.060	0.010	0.013	0.010	0.475	0.66	100667	0.034	61
5	0.014	0.045	0.0026	0.035	0.053	0.009	0.010	0.008	0.462	0.70	82667	0.034	61
6	0.014	0.059	0.0020	0.043	0.065	0.010	0.015	0.012	0.483	0.64	113333	0.034	61
7	0.014	0.061	0.0019	0.045	0.067	0.021	0.016	0.013	0.487	0.63	119333	0.034	61
8	0.014	0.045	0.0026	0.035	0.053	0.019	0.010	0.008	0.462	0.70	82667	0.034	61
9	0.014	0.051	0.0023	0.039	0.058	0.022	0.012	0.010	0.472	0.67	96000	0.034	61
10	0.014	0.062	0.0019	0.045	0.068	0.023	0.016	0.013	0.487	0.63	120000	0.034	61
11	0.014	0.056	0.0021	0.042	0.063	0.016	0.014	0.011	0.480	0.65	108000	0.034	61
12	0.014	0.044	0.0027	0.035	0.052	0.014	0.009	0.008	0.460	0.70	80667	0.034	61

3 Results

The longitudinal water surface and bed profiles measured along the centreline at the end of each test were represented in graphs [4] as in Figure 4, relative to test 6, where x is the longitudinal abscissa starting from the inlet.

In the upstream reach the normal flow depth, h_u, was also determined as the distance between the approximately parallel bed and water surface profiles. The maximum scour depth, y_s, the scour length, l_s, and the sill step, a_2, occurring upstream of the second sill, were also obtained from the bed profiles. The scour length was determined as the distance between the first sill and the point downstream of the scour hole where the slope seemed to reach a constant value. All results are shown in Table 3. The comparison between measured and calculated values of flow depth, sill step and dimensionless ratio a_2/h_u are shown in Figures 5–7. The agreement between measured and calculated flow depths is satisfactory, even if it is generally underestimated with Eq. (5) (Figure 5), probably due to uncertainties about values of the Manning roughness coefficient and the critical Shields mobility parameter. The new data lies in a range not previously covered by Gaudio *et al.* [5], but confirms the already observed behaviour (Figure 5). The comparison between measured and calculated values of the sill step, for both Eqs. (3) and (4), is also in accordance with data by Gaudio *et al.* [5] (Figure 6). Dimensionless values of the ratio a_2/h_u confirm that Eq. (4) can be preferred to Eq. (3) for a_2/h_u up to 0.15 (Figure 7).

Table 3 Measured quantities.

Test	h_u (m)	y_s (m)	l_s (m)	a_2 (m)
1	0.050	0.084	1.25	0.008
2	0.065	0.097	1.65	0.015
3	0.050	0.071	1.35	0.008
4	0.062	0.068	1.47	0.012
5	0.050	0.058	1.43	0.009
6	0.071	0.083	1.25	0.013
7	0.070	0.095	1.90	0.013
8	0.050	0.087	1.50	0.011
9	0.060	0.102	1.55	0.011
10	0.070	0.110	1.63	0.020
11	0.065	0.084	1.98	0.015
12	0.060	0.069	1.52	0.012

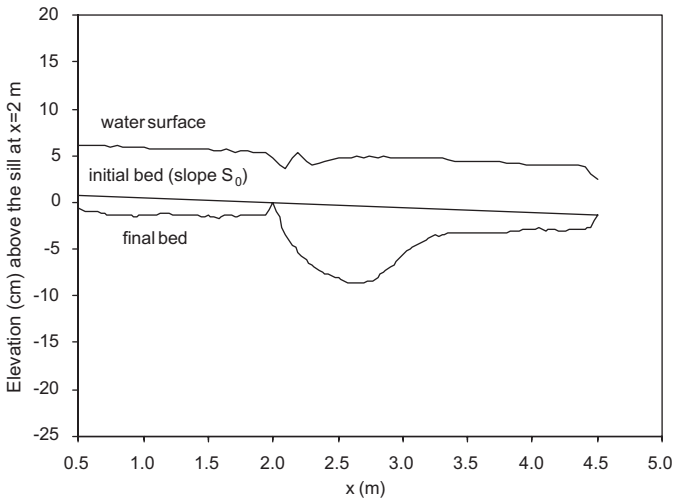

Figure 4 Water surface and bed profiles measured along the centreline (test 6).

The dimensionless parameters which are involved in Eqs. (1) and (2) were computed and presented in Table 4. Figure 8 shows a good agreement between Eq. (1) and the new set of points. Due to the presence of this new data, the following relation was derived with the least square linear regression to substitute the previous one (1):

$$\frac{y_s}{H_s} = 0.180\frac{a_1}{\Delta D_{50}} + 0.369, \tag{7}$$

valid in the range $1.3 \leq a_1/(\Delta D_{50}) \leq 9.1$, with a correlation coefficient $r = 0.94$.

Nevertheless, the new set of experimental data on scour length contrasts strongly with Eq. (2), as shown in Figure 9. As observed

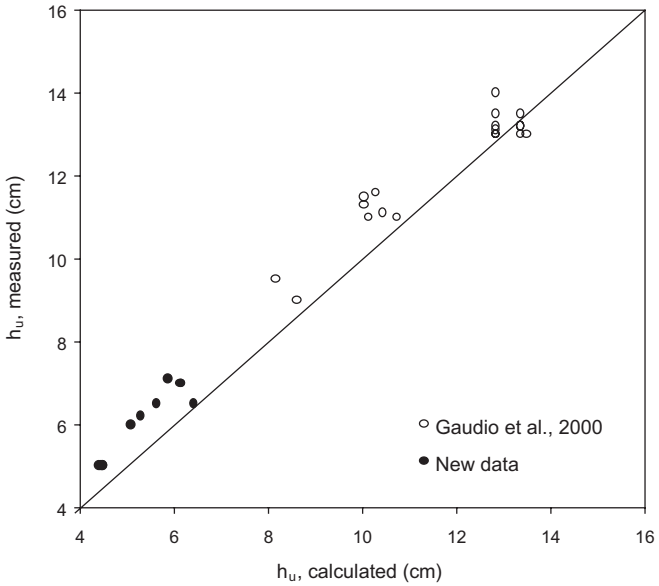

Figure 5 Comparison of measured and calculated flow depths.

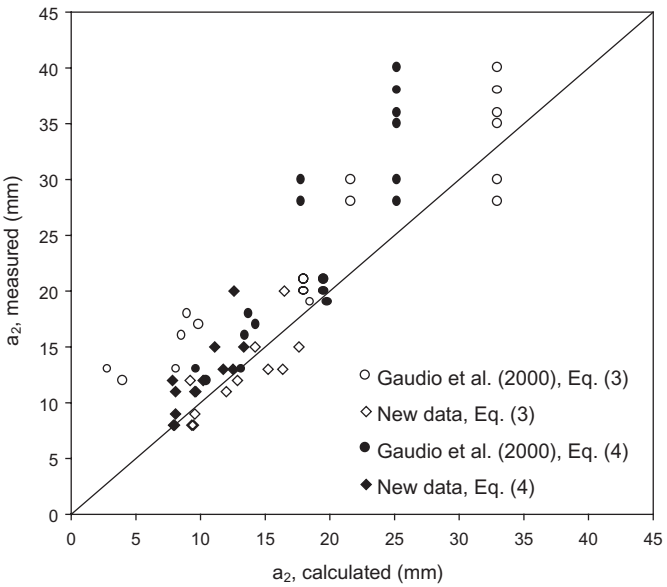

Figure 6 Comparison of measured and calculated sill steps.

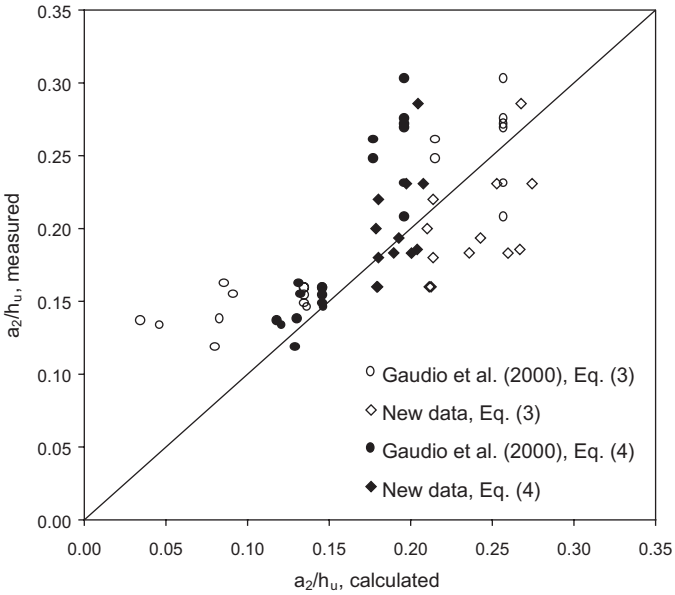

Figure 7 Comparison of measured and calculated non-dimensional a_2/h_u ratios.

Table 4 Non-dimensional parameters.

Test	$a_1/(\Delta D_{50})$	y_s/H_s	l_s/H_s
1	5.7	1.6	23.9
2	4.4	1.4	23.6
3	3.8	1.4	25.7
4	3.5	1.1	24.4
5	3.0	1.1	27.1
6	3.3	1.3	19.2
7	7.1	1.4	28.2
8	6.5	1.6	28.4
9	7.4	1.7	26.6
10	7.7	1.6	24.1
11	5.4	1.3	31.4
12	4.9	1.3	29.3

during the experimental tests and confirmed with the successive video-tape analysis, the length of the scour hole seemed to increase slowly but continuously, in spite of the fact that a stable value of y_s had already been reached after a few hours. This might be explained with the following considerations:

(a) it was observed that the pump worked with pulsations, producing discharge oscillations; these instabilities determined instantaneous velocity and shear stress values at the bottom greater than the ones associated with steady flow. As a matter of fact, this did not affect the scour depth, probably dominated by the dynamics of the hydraulic jump that dampened the perturbations;

(b) a weaker effect may have been produced due to the presence of glass panels on the sides of the duct, in particular in the local scouring region, which may have caused a reduction in the effective roughness value, with consequences analogous to the above ones.

Similar problems did not occur in the tests performed in the *Tilting Flume* at HR Wallingford Ltd., from which (1) and (2) were obtained [5]; it is believed, therefore, that the values of l_s are not meaningful, even if doubts remain about the possibility that the scour length can follow laws different from (2) in the case of sand.

The plot of dimensionless scour hole profiles is shown in Figure 10, where y is the scour depth at the abscissa x_1 starting from the first sill. Normalised scour hole profiles are affine, falling in a narrow band, as already found by Gaudio *et al.* [5] and other Authors for analogous scouring processes [7,12]. The maximum scour depth occurred at $x_1/l_s = 0.30$–0.40.

Image analysis was performed to obtain water surface and bed profiles over time at the left glass panel of the duct. Starting from the recorded video-cassettes, images were grabbed with proper software (*ATI Player* ©) into a PC at given time intervals and analysed with *Autocad 14* ©. A variable time step was adopted to describe the first hours of the scouring process more carefully,

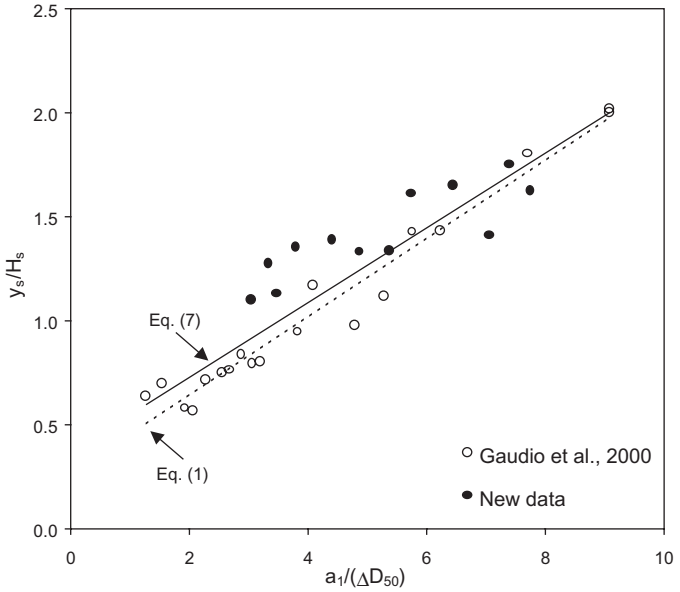

Figure 8 Dimensionless final maximum scour depths (centreline).

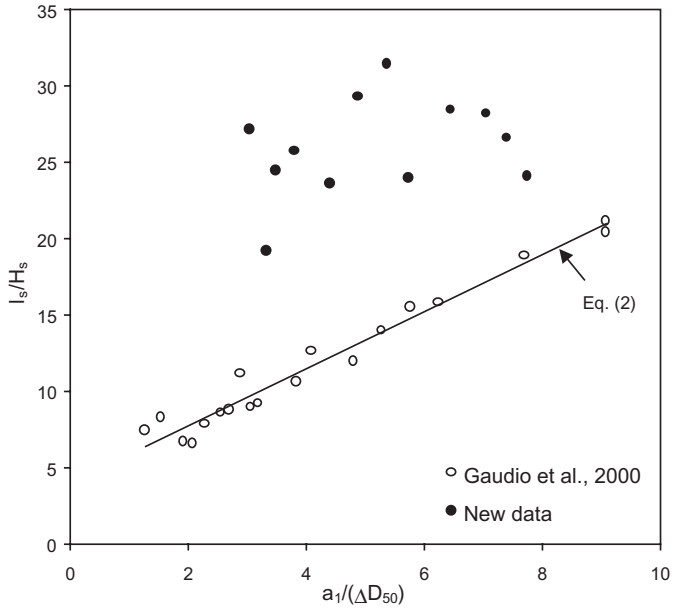

Figure 9 Dimensionless final scour lengths (centreline).

when the evolution of the scour hole is the quickest. Digitised profiles were interpolated with spline functions (polynomial function of given order, m, that assume the value of the co-ordinates of the data points and are completely determined with the continuity conditions of the derivatives of order $1, 2, \ldots, m-1$ at the mesh-points and with boundary conditions) and, then, rendered as sets of points in the Cartesian plane. Each point set was plotted and for each test a graph showing all the profiles over time was obtained [4] (e.g., Figure 11 for test 1). All the profiles over the horizontal line crossing the origin represent the water surface and the remaining profiles represent the bed. They obviously show that the scour hole dimensions increased over time. It was not possible to detect points in proximity of the section at $x = 2.5$ m from the images, due to the presence of the metal support of the central glass panel (see Figure 2 and, more clearly, the following Figures 12).

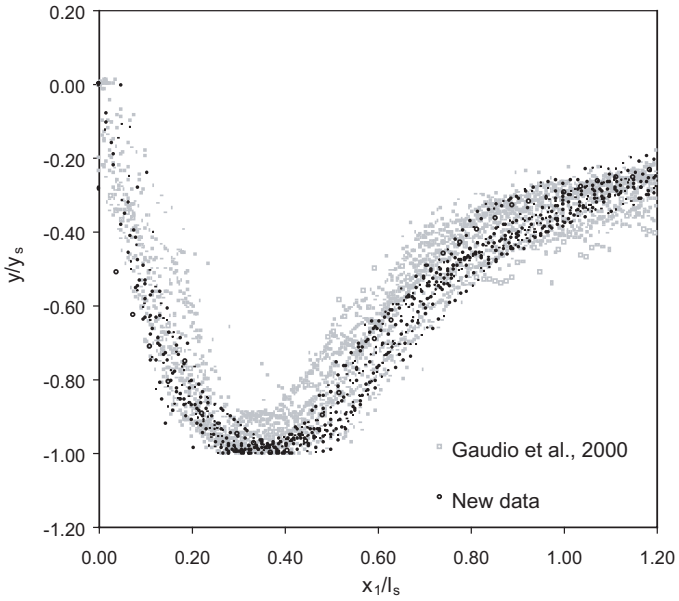

Figure 10 Dimensionless plot of scour hole profiles (centreline).

Sometimes an instantaneous scour depth, $y_s(t)$, greater than the equilibrium depth, y_s, occurred. Analogous phenomena were observed by Clarke [1] – who called $y_s(t)$ "dynamic depth" and y_s "static depth" –, Farhoudi and Smith [3] and Mohamed and McCorquodale [11]. This phenomenon, lasting about half an hour, happened with chaotic features at the end of the experiment. The achieved equilibrium conditions were perturbed and the scour hole dimensions downstream of the first sill increased. A sort of hillock of deposited sediments took place in the scour hole. Secondary currents, vortexes with a vertical rotation axis and sediment transport from downstream to upstream were observed. The flow destroyed the deposit after a certain time and the previously existing equilibrium conditions were re-established. It is not easy to give an exhaustive explanation of the above-described perturbation phenomenon. It is possible to hypothesise that an instability of the discharge raised up by the pump may have influenced the flow jet on the sill. Local velocity and bottom shear stress values may have consequently increased, causing sediment motion for some moments, even if the equilibrium conditions had already been reached. A photographic sequence of the chaotic phenomenon that happened during test 7 is shown in Figures 12a–f. In test 9, after the equilibrium conditions had been established, it was observed that the perturbation phenomenon occurred cyclically, with a period of the order of 1 h.

It is interesting to study the development of the maximum scour depth over time. Table 5 shows the time, t, measured starting from the beginning of each run and the corresponding maximum scour depth, $y_s(t)$. Figure 13 shows the experimental data: for each test the time evolution of y_s is qualitatively exponentially decreasing. In an attempt at finding common behaviour to all the data sets, which seem to obey a unique law, the instantaneous maximum scour depth, $y_s(t)$, was divided by the average equilibrium scour depth after 20 h, $\bar{y}_{s(t\geq 20\,\mathrm{h})}$ (Table 5). This average value was considered to take into account that the "dynamic" depth was sometimes greater than the "static" depth at equilibrium. In addition, it is to be noticed that in the present work the

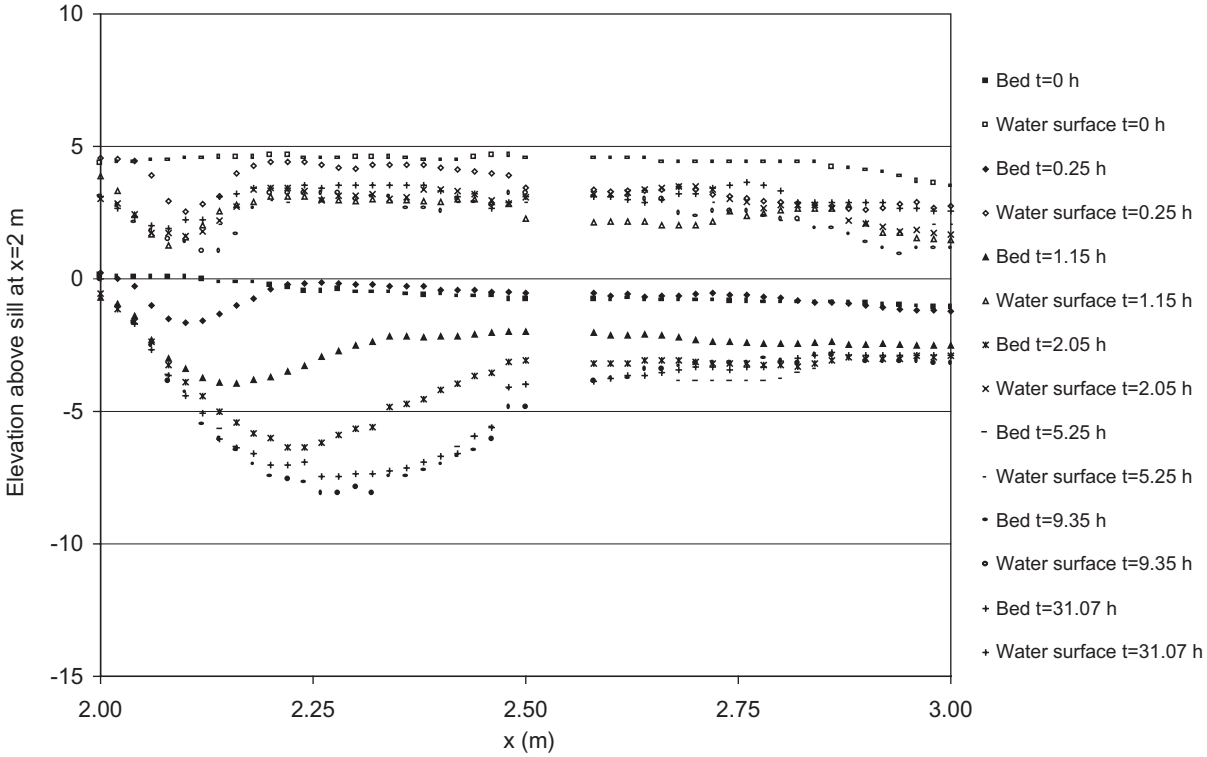

Figure 11 Test 1, temporal evolution of water surface and scour hole profiles (left side).

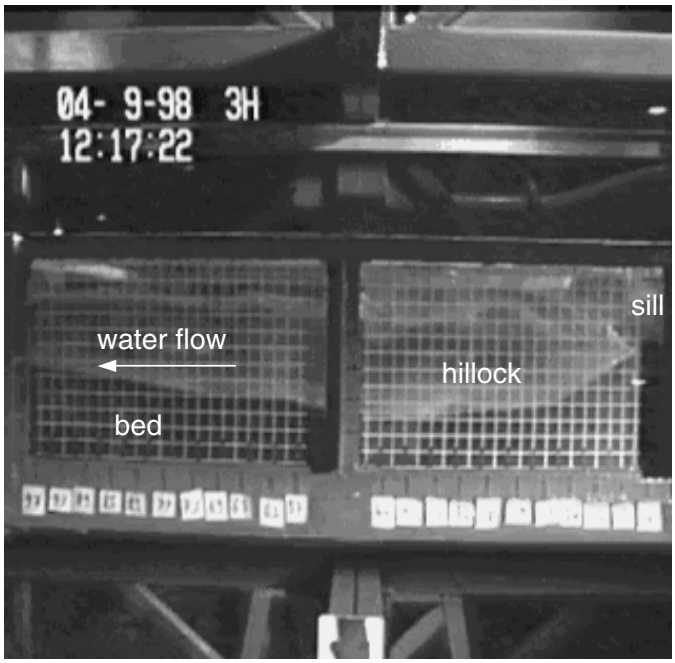

Figure 12a Perturbation phenomenon starting in the scour hole (test 7).

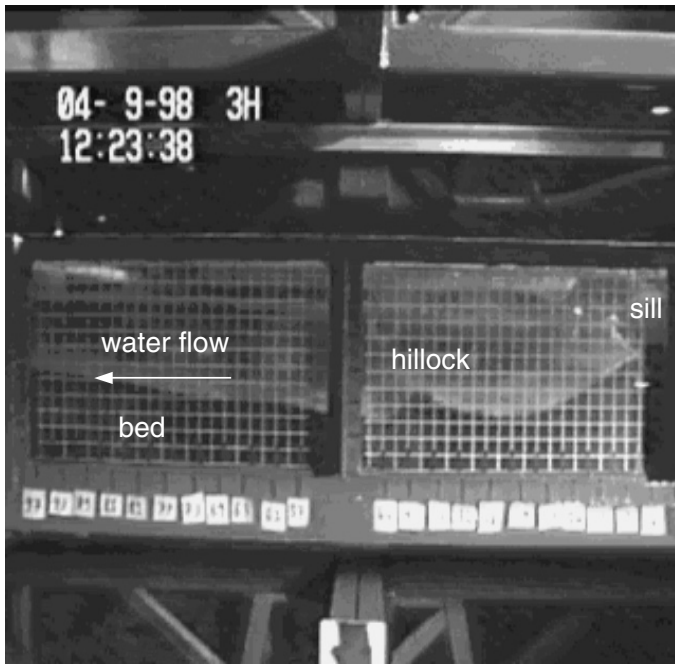

Figure 12b Perturbation phenomenon in the scour hole: hillock formation (test 7).

long-term values of the scour depth, y_s, given by Eqs. (1) and (7), were measured along the centreline, while the values of $y_s(t)$ – and, consequently, $\bar{y}_{s(t\geq 20\,\mathrm{h})}$ – were measured at the left side of the duct. The values of the dimensionless ratio:

$$y^* = \frac{y_s(t)}{\bar{y}_{s(t\geq 20\,\mathrm{h})}} \tag{8}$$

are shown in Table 5 and its temporal evolution is represented in Figure 14, where the initial, quick phase of erosion (short-term local scouring) is clearly distinguishable from the final, slow phase (long-term local scouring) tending to equilibrium.

This result can be improved introducing a dimensionless ratio also in the abscissa. The "hydraulic" time, t, can be divided by a "morphological" time, t_s, given by the ratio between an eroded volume and a sediment discharge. The morphological time was computed with the following procedure:

- the liquid discharge per unit width, q, is known;
- the initial bed slope, S_0, is known;

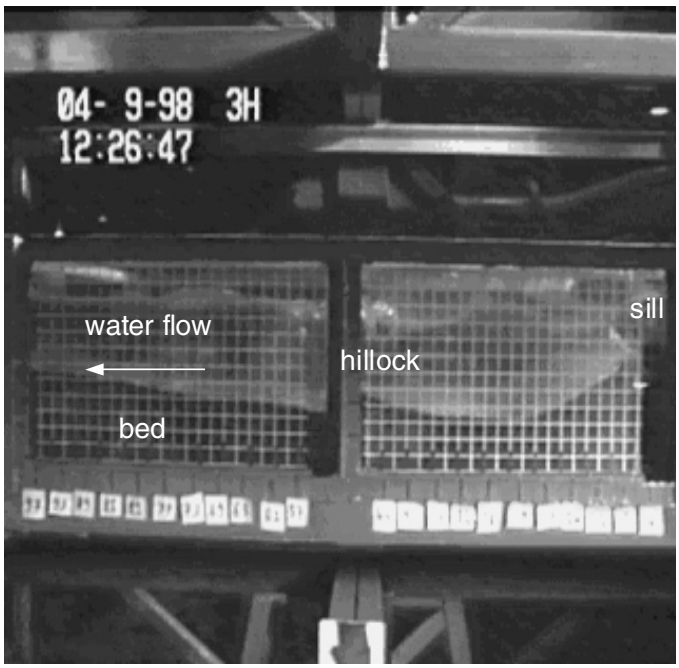

Figure 12c Perturbation phenomenon in the scour hole: hillock migration (test 7).

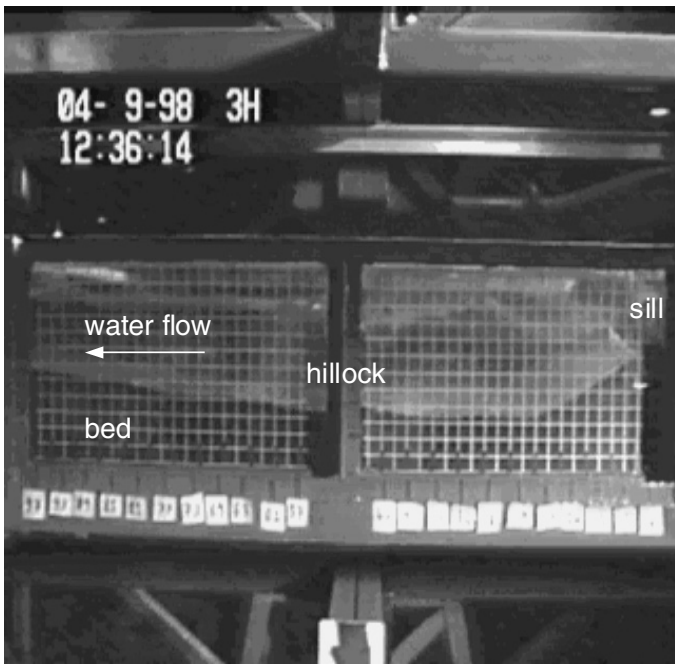

Figure 12e Perturbation phenomenon in the scour hole: hillock migration (test 7).

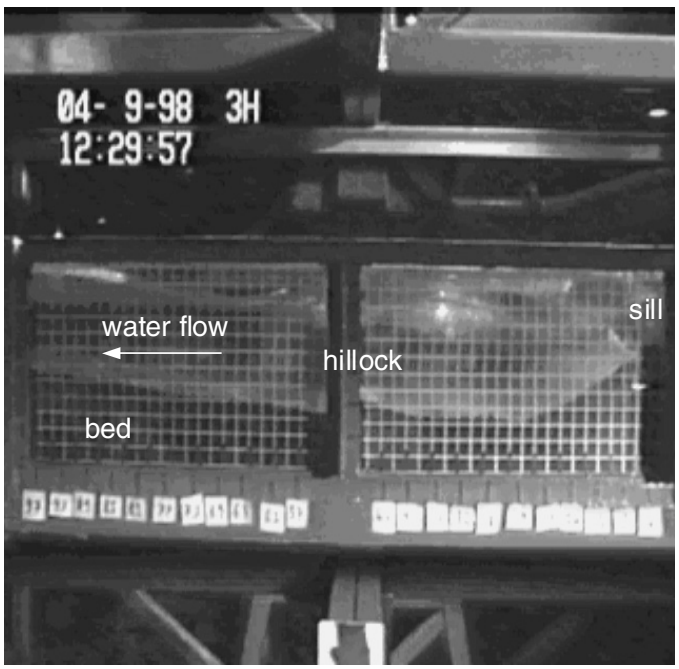

Figure 12d Perturbation phenomenon in the scour hole: hillock migration (test 7).

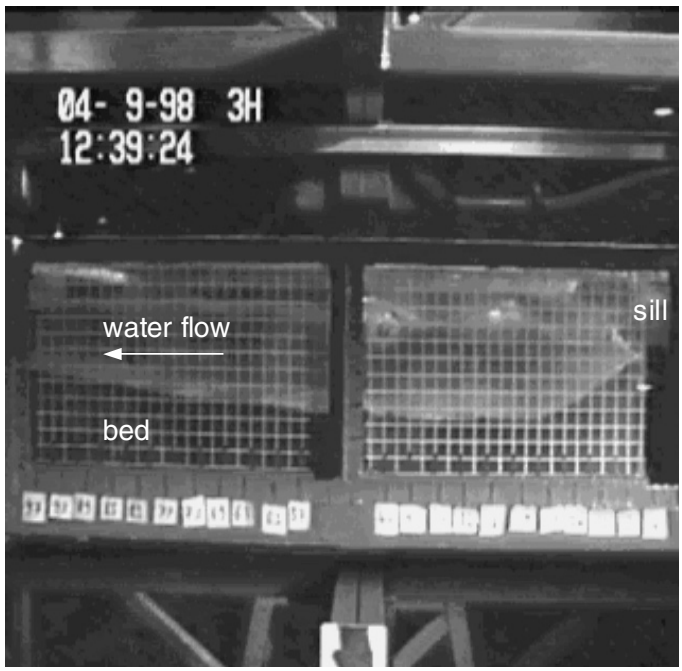

Figure 12f Perturbation phenomenon in the scour hole: hillock disappearance (test 7).

- the initial flow depth is given by the Manning formula [9]:

$$h = \left(\frac{nq}{S_0^{1/2}} \right)^{3/5} ; \tag{9}$$

- assuming the Shields critical mobility parameter $\Theta_c = 0.040$, the dimensionless initial sediment discharge can be evaluated by the Meyer-Peter and Müller formula [10]:

$$\Phi = 8 \left(\frac{hS_0}{\Delta D_{50}} - \Theta_c \right)^{3/2} ; \tag{10}$$

- the initial volumetric sediment discharge per unit width is [10]:

$$q_s = \Phi \sqrt{g \Delta D_{50}^3}; \tag{11}$$

- neglecting the area of the localised scour hole and considering that the bed upstream to the first sill (reach for $x = 0.0$–2.0 m, with length $L_u = 2.0$ m) and downstream of it (reach for $x = 2.0$–4.5 m, with length $L = 2.5$ m) experiences a roto-translation (see Figure 1 with a_1 and a_2), the scouring area is:

$$A_s = L_u \left(\frac{a_1 L_u}{2L} + a_2 \right) + L \left(\frac{a_1}{2} + a_2 \right), \tag{12}$$

Table 5 Temporal evolution of maximum scour depth (left side).

Test 1				Test 2				Test 3				Test 4				Test 5				Test 6			
t (h)	$y_s(t)$ (cm)	t^*	y^*	t (h)	$y_s(t)$ (cm)	t^*	y^*	t (h)	$y_s(t)$ (cm)	t^*	y^*	t (h)	$y_s(t)$ (cm)	t^*	y^*	t (h)	$y_s(t)$ (cm)	t^*	y^*	t (h)	$y_s(t)$ (cm)	t^*	y^*
0.00	0.00	0.000	0.00	0.00	0.00	0.000	0.00	0.00	0.00	0.000	0.00	0.00	0.00	0.000	0.00	0.00	0.00	0.000	0.00	0.00	0.00	0.000	0.00
0.42	1.65	0.685	0.20	0.50	2.52	0.745	0.30	0.50	2.08	0.625	0.32	0.50	1.48	0.523	0.19	0.50	1.61	0.462	0.25	0.50	1.69	0.525	0.23
0.84	3.54	1.371	0.42	1.00	4.48	1.490	0.53	1.00	2.68	1.251	0.42	1.00	2.67	1.045	0.35	1.00	2.38	0.925	0.37	1.00	2.00	1.050	0.27
1.26	3.95	2.056	0.47	1.50	5.93	2.235	0.70	1.50	3.88	1.876	0.60	1.33	2.93	1.390	0.38	1.50	2.90	1.387	0.45	1.50	2.22	1.575	0.30
1.67	5.10	2.741	0.61	2.00	7.18	2.980	0.84	2.00	5.69	2.502	0.88	2.00	3.14	2.091	0.41	2.00	2.90	1.850	0.45	2.00	2.68	2.101	0.37
2.09	6.36	3.426	0.76	2.50	7.83	3.725	0.92	2.50	5.69	3.127	0.88	2.50	3.42	2.613	0.45	2.50	3.01	2.312	0.47	2.50	3.02	2.626	0.41
2.51	6.33	4.112	0.76	3.00	7.83	4.470	0.92	3.00	5.24	3.753	0.81	3.00	4.33	3.136	0.57	3.00	3.11	2.775	0.49	3.00	3.13	3.151	0.43
2.93	6.78	4.797	0.81	3.50	7.61	5.215	0.90	3.50	5.69	4.378	0.88	3.50	4.45	3.659	0.58	3.50	3.64	3.237	0.57	3.50	3.53	3.676	0.48
3.35	7.08	5.482	0.85	4.00	7.61	5.980	0.90	4.00	5.69	5.004	0.88	4.00	4.86	4.181	0.63	4.00	3.43	3.699	0.54	4.00	3.78	4.201	0.51
3.77	6.91	6.168	0.83	4.50	8.05	6.705	0.95	4.50	5.99	5.629	0.93	4.50	4.96	4.704	0.65	4.50	3.96	4.162	0.62	4.50	3.81	4.726	0.52
4.18	7.40	6.853	0.89	5.00	7.51	7.451	0.88	5.00	6.44	6.255	1.00	5.00	4.92	5.227	0.64	5.00	3.96	4.624	0.62	5.00	4.04	5.252	0.55
4.60	7.58	7.538	0.91	7.00	8.38	10.431	0.98	7.00	6.14	8.756	0.95	7.00	5.44	7.317	0.71	7.00	4.59	6.474	0.72	7.00	4.38	7.352	0.60
5.02	7.48	8.223	0.90	9.00	9.61	13.411	1.13	9.00	6.89	11.258	1.07	9.00	6.31	9.408	0.82	10.00	4.91	9.248	0.77	9.00	4.83	9.453	0.66
5.44	7.54	8.909	0.90	11.00	8.97	16.391	1.05	11.00	6.89	13.760	1.07	11.00	6.58	11.498	0.86	12.00	5.23	11.098	0.82	11.00	5.17	11.553	0.71
5.86	7.54	9.594	0.90	13.00	9.39	19.371	1.10	13.00	7.19	16.262	1.11	13.00	6.56	13.589	0.86	14.00	6.61	12.948	1.03	13.00	5.75	13.654	0.79
6.28	7.57	10.279	0.91	15.00	9.09	22.352	1.07	15.00	7.04	18.764	1.09	15.00	6.88	15.680	0.90	16.00	5.55	14.797	0.87	15.00	6.21	15.755	0.85
6.69	7.57	10.965	0.91	20.00	8.30	29.802	0.98	20.00	7.04	25.018	1.09	20.00	7.88	20.906	1.03	20.00	5.97	18.497	0.93	20.00	6.77	21.006	0.93
7.11	7.72	11.650	0.93	25.00	8.07	37.253	0.95	25.00	7.34	31.273	1.14	25.00	7.43	26.133	0.97	25.00	6.29	23.121	0.96	25.00	7.00	26.258	0.96
7.53	7.42	12.335	0.89	30.00	8.42	44.703	0.99	30.00	7.49	37.528	1.16	30.00	7.65	31.359	1.00	30.00	6.06	27.745	0.95	30.00	7.34	31.509	1.00
9.62	8.10	15.762	0.97	35.00	8.42	52.154	0.99	66.00	6.14	82.561	0.95	35.00	7.79	36.586	1.02	35.00	6.48	32.369	1.01	35.00	7.23	36.761	0.99
11.30	8.26	18.503	0.99	40.00	8.41	59.604	0.99	71.00	5.99	88.815	0.93	40.00	7.73	41.812	1.01	40.00	6.59	36.994	1.03	40.00	7.23	42.012	0.99
12.97	8.33	21.244	1.00	50.00	8.52	74.505	1.00	85.00	5.54	106.328	0.86	45.00	7.45	47.039	0.97	50.00	6.65	46.242	1.04	50.00	7.48	52.515	1.02
15.06	8.68	24.670	1.04	60.00	8.73	89.406	1.03	88.65	5.69	110.894	0.88					60.00	6.46	55.490	1.01	60.00	7.59	63.018	1.04
20.08	8.61	32.894	1.03	70.00	9.17	104.307	1.08									69.00	6.75	63.814	1.05	70.00	7.82	73.521	1.07
25.00	8.76	40.947	1.05																				
31.00	7.46	50.774	0.89																				
35.00	9.13	57.326	1.09																				
40.00	9.11	65.515	1.09																				
51.00	8.73	83.532	1.05																				
60.00	8.17	98.272	0.98																				
73.00	8.02	119.565	0.96																				
82.40	7.83	134.961	0.94																				
88.00	7.66	144.133	0.92																				
$\bar{y}_{s(t\geq 20\,\mathrm{h})}$ (cm)		8.35			8.51				6.46				7.65				6.41				7.31		

Table 5 Continued.

Test 7				Test 8				Test 9				Test 10				Test 11				Test 12			
t (h)	$y_S(t)$ (cm)	t^*	y^*	t (h)	$y_S(t)$ (cm)	t^*	y^*	t (h)	$y_S(t)$ (cm)	t^*	y^*	t (h)	$y_S(t)$ (cm)	t^*	y^*	t (h)	$y_S(t)$ (cm)	t^*	y^*	t (h)	$y_S(t)$ (cm)	t^*	y^*
0.00	0.00	0.000	0.00	0.00	0.00	0.000	0.00	0.00	0.00	0.000	0.00	0.00	0.00	0.000	0.00	0.00	0.00	0.000	0.00	0.00	0.00	0.000	0.00
0.50	3.97	1.158	0.39	0.50	5.49	0.814	0.62	0.50	8.21	1.039	0.70	0.50	8.24	0.960	0.64	0.50	2.14	0.744	0.26	0.50	2.07	0.589	0.31
1.00	8.67	2.316	0.85	1.00	8.44	1.628	0.95	1.00	9.64	2.078	0.82	1.00	12.26	1.921	0.95	1.00	3.22	1.489	0.39	1.00	3.13	1.139	0.47
1.50	9.32	3.474	0.91	1.50	7.89	2.443	0.86	1.50	11.08	3.117	0.94	1.50	12.93	2.881	1.00	1.50	4.82	2.233	0.59	1.50	4.97	1.708	0.74
2.00	9.54	4.632	0.93	2.00	7.49	3.257	0.84	2.00	10.11	4.156	0.86	2.00	11.65	3.842	0.90	2.00	5.59	2.977	0.68	2.00	5.71	2.277	0.86
2.50	9.64	5.790	0.94	2.50	7.38	4.071	0.83	2.50	10.65	5.195	0.91	2.50	13.25	4.802	1.03	2.50	6.44	3.722	0.78	2.50	6.25	2.847	0.94
3.00	9.64	6.948	0.94	3.00	7.82	4.885	0.88	3.00	11.53	6.234	0.98	3.00	12.21	5.763	0.95	3.00	5.69	4.466	0.69	3.00	6.36	3.416	0.95
3.50	9.75	8.106	0.96	3.50	7.82	5.700	0.88	3.50	10.76	7.274	0.92	3.50	12.10	6.723	0.94	3.50	7.20	5.211	0.87	3.50	6.41	3.986	0.96
4.00	10.08	9.264	0.99	4.00	8.58	6.514	0.96	4.00	10.54	8.313	0.90	4.00	12.42	7.683	0.96	4.00	8.17	5.955	0.99	4.00	6.56	4.555	0.98
4.50	9.43	10.422	0.92	4.50	8.47	7.328	0.95	4.50	10.76	9.352	0.92	4.50	12.47	8.644	0.97	4.50	7.63	6.699	0.93	4.50	6.47	5.124	0.97
5.00	10.30	11.580	1.01	5.00	8.47	8.142	0.95	5.00	11.20	10.391	0.95	5.00	12.37	9.604	0.96	5.00	7.95	7.444	0.96	5.00	6.47	5.694	0.97
7.00	10.73	16.212	1.05	7.00	8.58	11.399	0.96	7.00	10.87	14.547	0.93	7.00	13.00	13.446	1.01	7.00	7.63	10.421	0.93	7.00	6.47	7.971	0.97
9.00	10.20	20.844	1.00	9.00	8.80	14.656	0.99	9.00	11.06	18.703	0.94	9.00	11.84	17.288	0.92	9.00	7.74	13.399	0.94	9.00	6.75	10.249	1.01
11.00	9.40	25.476	0.92	11.00	8.80	17.913	0.99	11.00	11.61	22.880	0.99	11.00	12.26	21.129	0.95	11.00	8.22	16.376	1.00	11.00	6.43	12.526	0.96
13.00	10.16	30.108	1.00	13.00	8.47	21.170	0.95	13.00	10.84	27.016	0.92	13.00	12.37	24.971	0.96	13.00	8.22	19.353	1.00	13.00	6.43	14.804	0.96
15.00	9.96	34.741	0.98	15.00	8.89	24.427	1.00	15.00	11.09	31.172	0.94	15.00	12.58	28.813	0.98	15.00	8.11	22.331	0.98	15.00	6.75	17.081	1.01
20.00	9.85	46.321	0.96	20.00	8.67	32.570	0.97	20.00	10.92	41.563	0.93	20.00	12.05	38.417	0.94	20.00	8.54	29.774	1.04	20.00	7.07	22.775	1.06
25.00	9.52	57.901	0.93	25.00	8.78	40.712	0.98	25.00	11.14	51.954	0.95	25.00	12.26	48.021	0.95	25.00	8.11	37.218	0.98	25.00	6.21	28.469	0.93
30.00	10.83	69.481	1.06	30.00	8.67	48.855	0.97	30.00	11.78	62.344	1.00	30.00	12.88	57.625	0.98	30.00	8.00	44.662	0.97	30.00	6.43	34.162	0.96
37.00	9.85	85.693	0.96	35.00	8.78	56.997	0.98	35.00	11.58	72.735	0.99	35.00	13.00	67.230	1.01	35.00	8.54	52.105	1.04	35.00	6.52	39.856	0.98
41.00	10.61	94.957	1.04	40.00	8.99	65.139	1.01	40.00	11.47	83.126	0.98	40.00	13.53	76.834	1.05	40.00	8.43	59.549	1.02	40.00	6.43	45.550	0.96
51.00	10.81	118.118	1.04	50.00	8.99	81.424	1.01	50.00	12.79	103.907	1.09	50.00	12.89	96.042	0.98	50.00	8.32	74.436	1.01	50.00	6.64	56.937	0.99
				60.00	9.32	97.709	1.04	60.00	12.46	124.689	1.06	59.00	13.11	113.330	1.02	60.00	8.54	89.323	1.04	57.00	6.53	64.909	0.98
				70.00	8.88	113.994	1.00					65.75	13.75	126.296	1.07	70.00	7.47	104.211	0.91	67.00	7.07	76.296	1.06
				89.00	9.21	114.935	1.03													77.00	6.96	87.684	1.04
																				90.00	6.91	102.487	1.03
$\bar{y}_{s(t\geq 20\,\mathrm{h})}$ (cm)		10.21			8.92				11.73				12.88				8.24				6.68		

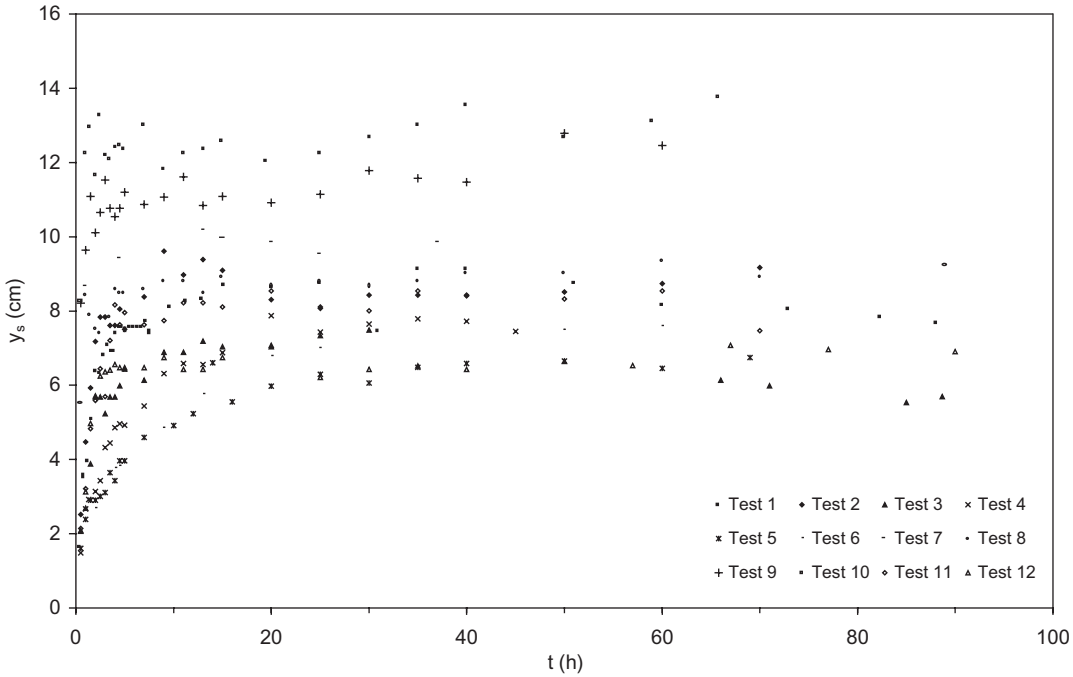

Figure 13 Exponentially decreasing temporal trend of maximum scour depth (left side).

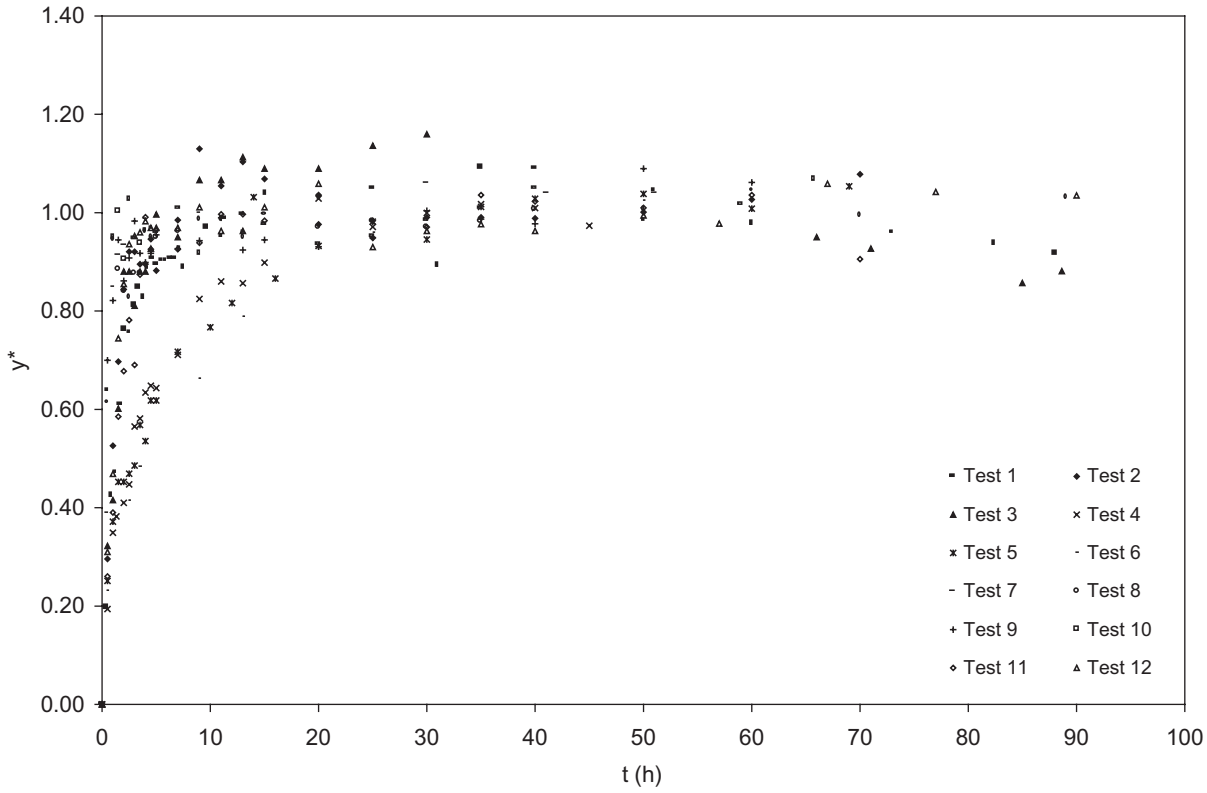

Figure 14 Temporal evolution of dimensionless maximum scour depth (left side).

where $a_1 L_u / L$ is an estimation of the morphological jump in the upstream reach;

- the morphological time is obtained as the ratio between the scouring area and the initial sediment discharge per unit width:

$$t_s = \frac{A_s}{q_s}. \tag{13}$$

For each test, the above procedure was applied and t_s was computed (Table 6).

The dimensionless time is given by:

$$t^* = \frac{t}{t_s}. \tag{14}$$

Figure 15 shows the evolution of y^* vs t^*, with an exponentially decreasing curve, fitting all the points, that collapse into a narrower band than in Figure 14. The short-term and long-term phases of the local scouring process are clearly distinguished.

Table 6 Morphological time computation.

Test	q (m^2/s)	S_0	h (m)	Φ	q_s (m^2/s)	a_1 (m)	a_2 (m)	A_s (m^2)	t_s (s)
1	0.020	0.0094	0.030	0.106	3.2E-05	0.017	0.008	0.071	2198
2	0.032	0.0070	0.043	0.128	3.9E-05	0.013	0.015	0.094	2416
3	0.021	0.0071	0.034	0.067	2.0E-05	0.011	0.008	0.059	2878
4	0.025	0.0063	0.039	0.071	2.2E-05	0.010	0.012	0.075	3444
5	0.021	0.0062	0.035	0.050	1.5E-05	0.009	0.009	0.059	3893
6	0.028	0.0059	0.042	0.075	2.3E-05	0.010	0.013	0.079	3428
7	0.030	0.0102	0.037	0.214	6.5E-05	0.021	0.013	0.102	1554
8	0.021	0.0102	0.030	0.131	4.0E-05	0.019	0.011	0.088	2211
9	0.024	0.0110	0.032	0.179	5.5E-05	0.022	0.011	0.095	1732
10	0.030	0.0110	0.036	0.240	7.3E-05	0.023	0.020	0.137	1874
11	0.027	0.0084	0.037	0.136	4.1E-05	0.016	0.015	0.100	2418
12	0.020	0.0084	0.031	0.086	2.6E-05	0.014	0.012	0.083	3161

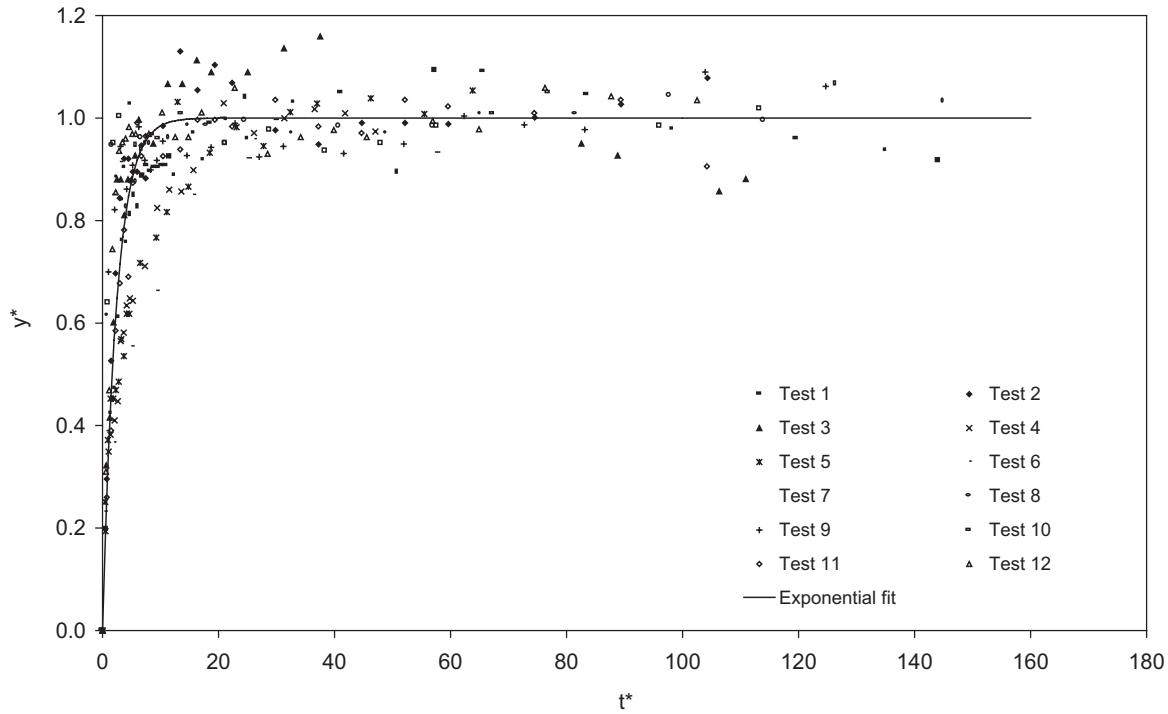

Figure 15 Dimensionless temporal evolution of maximum scour depth (left side).

The exponential fit law describing the curve is the following:

$$y^* = 1 - \exp(-0.418 \cdot t^*), \tag{15}$$

which is valid in the range $0 \leq t^* \leq 144.9$, with a correlation coefficient $r = 0.91$.

4 Discussion

Time evolution of local scouring downstream of bed sills was investigated with an experimental approach. An empirical law was obtained for the evaluation of the maximum scour depth at given time, particularly useful for investigations on short-term local scouring.

Conceptually, the instantaneous maximum scour depth, $y_s(t)$, is considered as a fraction of the maximum scour depth at equilibrium, y_s. A dimensional analysis of the problem of local scour at bed sills was presented in [5], leading to non-dimensional relations, as Eqs. (1) and (2), which are ready for use in prototype conditions. The temporal evolution described by Eq. (15) was also derived in non-dimensional terms. The variables are normalised with quantities that can be evaluated using scale-independent relationships, e.g. most transport formulae that respect dimensional considerations. For these reasons, the present results are supposed not to be affected by scale effects when applied to real cases. Nevertheless, limitations to the use of the obtained empirical formulae exist: the experiments dealt with not too high longitudinal bed slopes, uniform sediment, no armouring of the bed and no sediment feeding.

5 Conclusions

Time evolution of local scouring downstream of bed sills was investigated performing a set of 12 experimental tests in the *Sloping Sediment Duct* at HR Wallingford Ltd., in 1998. A uniform sand was used and no sediment was injected at the upstream end of the flume.

Results confirmed the validity of the method for the assessment of the long-term maximum depth of scour, y_s, proposed by Gaudio *et al*. [5]. Doubts arose about the estimation of the length of the scour hole, l_s.

The study of the temporal evolution of the maximum scour depth showed that the scour hole development is rapid and reaches values very close to those at equilibrium in a short time.

Non-dimensional variables, including a morphological time, t_s, permitted the description of temporal scour evolution with a unique exponentially decreasing curve. The short-term erosive phase is clearly distinguishable from the long-term phase.

The present research permitted the individuation of empirical relations which, in the investigated experimental range of values and for uniform sediment and no feeding, can be considered as valid for the assessment of the short- and long-term depth of the localised scour hole downstream of bed sills. In Appendix, an example of application shows how to evaluate the instantaneous maximum scour depth, $y_s(t)$. Further developments could involve high longitudinal bed slopes, non-uniform sediment with possible armouring of the bed and sediment feeding.

Acknowledgements

Funding for this work was provided by the Commission of the European Community's Directorate General for Science, Research and Development, as a part of the programme Training and Mobility of Researchers – Access to Large Scale Facilities, under Contract Number ERB FMGE CT95 0082.

Data analysis has been partially funded by the Italian Consiglio Nazionale delle Ricerche (CNR), Gruppo Nazionale per la Difesa dalle Catastrofi Idrogeologiche (GNDCI).

The authors would like to thank Leonardo Di Donna, Gianluca Giacometti, Elena Romano and Mattia Zaramella, who took part in carrying out the experiments; Enrico Cattini and Michael Keevil for the image analysis. Special thanks are due to Dr Roger Bettess of HR Wallingford Ltd. for valuable discussions. Two anonymous reviewers are gratefully acknowledged.

Appendix

An example of application of results to a practical case is shown. A rectangular channel is to be stabilised using bed sills, with spacing $L = 50$ m. The following data is known:

- width, $B = 113$ m;
- design discharge, $Q = 800\ \mathrm{m^3/s}$;
- initial bed slope, $S_0 = 0.0050$;
- relative submerged grain density, $\Delta = 1.63$;
- median sediment size, $D_{50} = 0.030$ m;
- grain size for which 90% by weight of the sediment is finer, $D_{90} = 0.090$ m.

What is the maximum scour depth at equilibrium and at the second sill after 2 h?

How long does it take to reach $y_s(t) = 1$ m?

Assuming a value of the critical Shields mobility parameter $\Theta_c = 0.040$, the following results are obtained:

- Manning's roughness coefficient: $n = 0.026\ \mathrm{s/m^{1/3}}$;
- discharge per unit width: $q = 7.1\ \mathrm{m^2/s}$;
- normal flow depth (Eq. (5)): $h_u = 3.37$ m;
- equilibrium slope (Eq. (6)): $S_{eq} = 0.0006$;
- critical flow depth: $h_c = 1.72$ m;
- critical specific energy: $H_s = 2.58$ m;
- mean velocity: $U = 2.10$ m/s;
- Froude number: $Fr = 0.37$;
- Reynolds number: $Re = 2.8 \cdot 10^7$;
- shear velocity: $u^* = 0.14$ m/s;
- shear Reynolds number: $Re^* = 4156$;
- morphological jump: $a_1 = 0.22$ m;
- dimensionless morphological jump: $a_1/(\Delta D_{50}) = 4.5$;
- maximum scour depth at equilibrium (Eq. (7)): $y_s = 3.1$ m;
- initial flow depth (Eq. (9)): $h = 1.77$ m;
- non-dimensional solid discharge (Eq. (10)): $\Phi = 0.42$;
- initial volumetric solid discharge per unit width (Eq. (11)): $q_s = 0.009\ \mathrm{m^2/s}$;
- sill step: $a_2 = h_u - h_c = 1.64$ m;
- scouring area (supposing an upstream reach length $L_u = L = 50$ m, Eq. (12)): $A_s = 175.5\ \mathrm{m^2}$;
- morphological time (Eq. (13)): $t_s = 20050$ s;
- dimensionless time (Eq. (14)): $t^*_{(t=2\,\mathrm{h})} = 0.36$;
- non-dimensional instantaneous maximum scour depth (Eq. (15)): $y^*_{(t=2\,\mathrm{h})} = 0.14$;
- maximum scour depth after 2 h (Eq. (8)): $y_{s(t=2\,h)} = y^* \cdot y_s = 0.43$ m;
- time needed to reach the maximum scour depth $y_s(t) = 1$ m (Eqs. (8), (14) and (15)):

$$t = t^*_{[y_s(t)=1\,\mathrm{m}]} \cdot t_s = -\frac{\ln\left[1 - (y_s(t)/y_s)\right]}{0.418} \cdot t_s = 5.28\,\mathrm{h}.$$

A better estimation of the sill step than that given by Eqs. (3) or (4) will exert a positive effect on the assessment of the short-term maximum scour depths. Anyway, the importance of the introduction of a_2 in the evaluation of the scouring area, A_s, is underlined, useful to reach the result shown in Figure 15 and, in particular, of Eq. (15).

Notations

$a_1 = (S_0 - S_{eq})L$ = morphological jump [L]
a_2 = sill step [L]
$a_{2,Reb}$ = sill step computed according to Rehbock's formula, Eq. (4) [L]
A_s = scouring area [$\mathrm{L^2}$]
B = width of the rectangular cross-section [L]

C_u = uniformity coefficient
D_{10} = grain size for which 10% by weight of the sediment is finer [L]
D_{50} = median grain size [L]
D_{60} = grain size for which 60% by weight of the sediment is finer [L]
D_{90} = grain size for which 90% by weight of the sediment is finer [L]
Fr = Froude number
g = gravity acceleration [L/T^2]
h = initial flow depth [L]
h_c = critical flow depth [L]
h_u = normal flow depth [L]
H_s = critical specific energy [L]
l_s = length of the scour hole [L]
L = distance between sills [L]
L_u = length of the reach upstream to the first sill [L]
m = polynomial order
n = Manning's roughness coefficient [T/L$^{1/3}$]
q = liquid discharge per unit width [L^2/T]
q_s = volumetric sediment discharge per unit width [L^2/T]
Q = liquid discharge [L^3/T]
r = correlation coefficient
Re = Reynolds number
Re^* = shear Reynolds number
S_0 = initial longitudinal bed slope
S_{eq} = equilibrium longitudinal bed slope
t = hydraulic time [T]
t_s = morphological time [T]
t^* = non-dimensional time
T = total duration of tests [T]
u^* = shear velocity [L/T]
U = mean velocity [L/T]
x = longitudinal abscissa starting from the inlet [L]
x_1 = longitudinal abscissa starting from the sill at x = 2 m [L]
y = scour depth [L]
y_s = maximum depth of the scour hole at equilibrium [L]
$\bar{y}_{s(t\geq 20\,\mathrm{h})}$ = average equilibrium depth of the scour hole for $t \geq 20$ h [L]
$y_s(t)$ = instantaneous maximum depth of the scour hole [L]
y^* = non-dimensional instantaneous maximum scour depth
Δ = relative submerged grain density
Θ_c = critical Shields' mobility parameter
ν = kinematic water viscosity [L^2/T]
ρ_s' = submerged grain density [M/L^3]
ρ_w = water density [M/L^3]
Φ = non-dimensional solid discharge

References

1. Clarke, F.R.W. (1962). "The Action of Submerged Jets on Moveable Material", Ph.D. Thesis, Imperial College, London, U.K.
2. Damgaard, J.S., Whitehouse, R.J.S. and Soulsby, R.L. (1996). "A Sloping Duct for the Study of Sediment Transport", *Proc. 25th International Conference on Coastal Engineering*, Orlando, Florida, 3913–3920.
3. Farhoudi, J. and Smith, K.V.H. (1985). "Local Scour Profiles Downstream of Hydraulic Jump", *J. Hydr. Res.* IAHR, 23(4), 343–358.
4. Gaudio, R. and Marion, A. (2000). "Time Evolution of Local Scouring at Bed Sills", Report TR69, HR Wallingford Ltd., Wallingford, U.K, 76 pp.
5. Gaudio, R., Marion, A. and Bovolin, V. (2000). "Morphological Effects of Bed Sills in Degrading Rivers", *J. Hydr. Res.* IAHR, 38(2), 89–96.
6. Ghetti, A. (1980). *Idraulica* (in Italian), 2nd edition, Cortina Editrice, Padua, Italy, 566 pp.
7. Habib, E., Mossa, M. and Petrillo, A. (1994). "Scour Downstream of Hydraulic Jump", *Modelling, Testing & Monitoring for Hydro Powerplants Conference*, Budapest, Hungary, 591–602.
8. Lambe, T.W. and Whitman, R.V. (1969). *Soil Mechanics*, SI version, 1978, John Wiley, New York, N.Y., p. 32.
9. Manning, R. (1891). "On the Flow of Water in Open Channels and Pipes", *Trans. Inst. Civ. Engrs. of Ireland*, Dublin, Ireland, 20, 161–207; supplement (1895), 24, 179–207.
10. Meyer-Peter, E. and Müller, R. (1948). "Formulas for Bed-Load Transport", *Second Meeting of the International Association for Hydraulic Research*, Stockholm, Sweden, 39–64.
11. Mohamed, M.S. and McCorquodale, J.A. (1992). "Short-term Local Scour", *J. Hydr. Res.* IAHR, 30(5), 685–699.
12. Rajaratnam, N. (1981). "Erosion by Plane Turbulent Jets", *J. Hydr. Res.* IAHR, 19(4), 339–358.
13. Shields, A. (1936). "Anwendung der Aehnlichkeitsmechanik und der Turbulenzforschung auf die Geschiebebewegung", *Mitteilungen der Preussischen Versuchsanstalt fur Wasserbau und Schiffbau*, Berlin, Germany, English translation *Application of Similarity Principles and Turbulence Research to Bed-Load Movement*, by W.P. Ott and J.C. van Uchelen, Soil Conservation Service, Cooperative Laboratory, California Institute of Technology, Pasadena, California.